ACS APPLIED MATERIALS & INTERFACES
Research Article
www.acsami.org

Interface Engineered $BaTiO_3/SrTiO_3$ Heterostructures with Optimized High-Frequency Dielectric Properties

Ming Liu,[†,‡] Chunrui Ma,[‡] Gregory Collins,[‡] Jian Liu,[‡] Chonglin Chen,[‡,*] Chao Dai,[§] Yuan Lin,[§] Li Shui,[†] Feng Xiang,[†] Hong Wang,[†] Jie He,[#] Jiechao Jiang,[#] Efstathios I. Meletis,[#] and Melanie W Cole[⊥]

[†]Electronic Materials Research Laboratory, Key Laboratory of the Ministry of Education and International Center for Dielectric Research, Xi'an Jiaotong University, Xi'an 710049, P. R. China

[‡]Department of Physics and Astronomy, University of Texas at San Antonio, San Antonio, Texas 78249, United States

[§]State Key Laboratory of Electronic Thin films and Integrated Devices, University of Electronic Science & Technology of China, Chengdu, Sichuan 610054, P. R. China

[#]Department of Materials Science and Engineering, University of Texas at Arlington, Arlington, Texas 76019, United States

[⊥]ARL U.S. Army Research Laboratory, WMRD, Rodman Materials Research Laboratory, Aberdeen Proving Ground, Maryland 21005, United States

ABSTRACT: Interface engineered $BaTiO_3/SrTiO_3$ heterostructures were epitaxially grown on (001) MgO substrates by pulsed laser deposition. Microstructural characterizations by X-ray diffraction and transmission electron microscopy indicate that the as-grown heterostructures are *c*-axis oriented with sharp interfaces. The interface relationships between the substrate and multilayered structures were determined to be $[001]_{SrTiO3}//[001]_{BaTiO3}//[001]_{MgO}$ and $(100)_{SrTiO3}//(100)_{BaTiO3}//(100)_{MgO}$. The high-frequency microwave (∼18 GHz) dielectric measurements reveal that the dielectric constant and dielectric loss of the nanolayered heterostructures are highly dependent upon the stacking period numbers and layer thicknesses. With the increase in the periodic number, or the decrease in each layer thickness, the dielectric constant dramatically increases and the dielectric loss tangent rapidly decreases. The strong interface effect were found when the combination period is larger than 16, or each STO layer is less than 6.0 nm. The optimized dielectric performance was achieved with the best value for the loss tangent (0.02) and the dielectric constant (1320), which suggests that the BTO/STO heterostructures be promising for the development of the room-temperature tunable microwave elements.

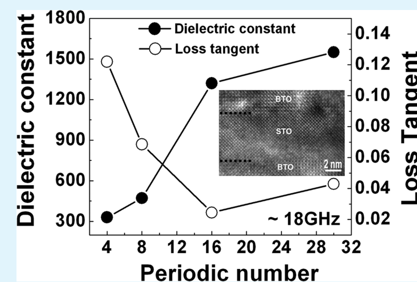

KEYWORDS: *BaTiO$_3$//SrTiO$_3$, heretostrctures, ferroelectric thin films, epitaxial behavior, microwave dielectric properties*

INTRODUCTION

Ferroelectric-perovskite oxide thin films have fascinated scientists and engineers' great attention because of their interesting physical properties and important application in various areas such as electric, optical, and microwave devices.[1−7] Especially, the nonlinear dielectric property has resulted in a significant increasing in the area of tunable wireless microwave communications, such as microwave tunable phase shifters, oscillators, filters, and antennas.[8−14] In the past two decades, ferroelectric Barium Strontium Titanate ($Ba_xSr_{1-x}TiO_3$ or BST) thin films have been considered to be one of the most important candidates for the microwave elements because of the tunable dielectric constant via an external field and adjustable curie temperature through varying the solution concentration between barium titanate and strontium titanate.[15,16] However, the relatively large dielectric insertion loss, soft mode effect, and limited figure of merit at high-frequency microwave region restrict the practical application in tunable microwave elements. Therefore, many techniques have been developed to improve the microwave dielectric properties, both in lowering down the loss-tangent and enhancing the tunability.[17−20] For instance, BTO and BST thin films have been systematically studied at 10 GHz with a dielectric loss 0.1.[21] Furthermore, Cole et al. demonstrated that the compositional gradient BST multilayers can significantly change the dielectric performance with the dielectric loss of ∼0.08, ∼0.06, ∼0.012 at 0.5, 5, and 10 GHz, respectively.[22] It has been also demonstrated that the Mn doped BST films can have the excellent dielectric properties with the average dielectric loss of 0.03 at a broad range high frequency from 15 GHz to 30 GHz is 0.033.[23]

Recently, the multifunctional tuning ferroelectric $BaTiO_3/SrTiO_3$ (BTO/STO) artificial multilayers and superlattices have been studied extensively because of their unique physical properties and phenomenon compared to the single-crystal films of BTO, STO, and BST. Previous research indicates that the size effects can significantly enhance the electric polarization, increase dielectric response, and dramatically change phase transition temperatures and other properties.[24−30] Especially, the previous studies on the BTO/STO multilayer

Received: June 13, 2012
Accepted: October 17, 2012
Published: October 17, 2012

ACS Publications © 2012 American Chemical Society

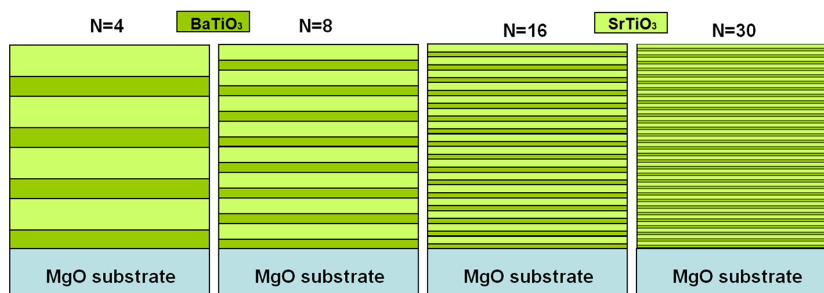

Figure 1. Sketch for the formula of BTO/STO superlattices structure.

systems indicate that the dielectric constant can be significantly enhanced at low-frequency range because of the large in-plane lattice mismatch of ∼3% between BTO (0.3990 nm) and STO (0.3905 nm) and the increase of interface strain with the increase of the period of the strained multilayered thin films.[31−35] However, the microwave dielectric properties of BTO/STO multilayered films in the range of GHz have not been reported yet. We have systematically studied the multilayered BTO/STO heterostructures and optimized the growth conditions to improve the high-frequency microwave dielectric properties and the corresponding physical properties. In this letter, we report the epitaxial behavior and high-frequency microwave dielectric properties of BTO/STO multilayered thin films on (001) MgO substrates.

EXPERIMENTAL SECTION

A KrF excimer pulsed laser deposition system with a wavelength of 248 nm with the energy density of about 2 J/cm^2 and a repetition rate of 4 Hz was employed to perform the fabrication of ferroelectric BTO/STO multilayered thin films on single-crystal (001) MgO substrates. Single-phase pure BTO and STO targets were used for the deposition. The single-crystal MgO substrates were selected for the epitaxial growth of the multilayered thin films because of its low frequency-dependent dielectric constant (∼9.7) and low loss tangent values (∼3.3 × 10^{-7}). In this system, the optimal growth conditions were found to be in the temperature higher than 840 °C with an oxygen pressure of 250 mTorr. The rate of the deposition time for the BTO and STO single-layer is 0.4 to 0.6 and the stacking periodic numbers are 4, 8, 16, and 30, respectively, as shown in the Figure 1, which gives the total film thickness of near 450 nm with the layer thickness of 6 nm and 9 nm for STO and BTO, respectively. All these samples were designed to have the same film thickness controlled with the equal total deposition time. The microstructure, crystallinity, and epitaxial behavior of the as-grown multilayered thin films were characterized by X-ray diffraction (XRD) and transmission electron microscopy (TEM). The microwave dielectric properties of the thin films were measured by split-post dielectric resonator technique at 18 GHz. The resonator was connected to the HP8720ES network analyzer. Using the software provided by the split-post dielectric resonators supplier (QWED), The dielectric constants ε and dielectric losses tan δ can be calculated from the equations described below[36,37]

$$\varepsilon = 1 + (f_0 - f_S)/hf_0K_\varepsilon(\varepsilon, h) \tag{1}$$

$$\tan\delta = (Q^{-1} - Q_{DR}{}^{-1} - Q_c{}^{-1})/P_{es} \tag{2}$$

Where the f_0 is empty resonator frequency, f_S is resonator frequency with sample, K_ε (ε, h) is obtained by the method of Rayleigh-Ritz, h is the thickness of sample, Q is the total quality factor, Q_{DR} is the quality factor of the dielectric resonator with sample, Q_c is the quality factor of metal resonator with sample, and P_{es} is the electromagnetism energy factor.

RESULTS AND DISCUSSION

Figure 2a shows the typical XRD patterns of the as-grown BTO/STO multilayered thin films deposited on (001) MgO

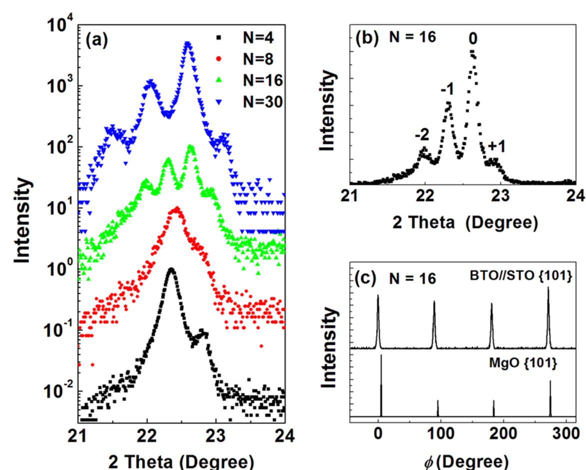

Figure 2. Typical X-ray diffraction pattern of the as-grown BTO/STO multilayered thin films deposited on (001) MgO substrates, (a) with a total deposition time but different N, (b) N = 16, (c) the ϕ scans taken along the ⟨101⟩ direction of the multilayered thin films and MgO substrates, displaying that the films are excellent epitaxial behavior.

substrates with a total deposition time of 40 min but different stacking periodic numbers (N). Only (00l) peaks appear in the θ−2θ scans for both thin films and substrates, indicating that the multilayered thin films have grown with c-axis perpendicular to the plane of the substrate. It can be clearly seen that the XRD patterns have two sets of peaks when the N is 4 or 8, one is from BTO and the other is from STO. With the increase of the N to 16, the satellite peaks appear. Figure 2b is the XRD pattern of the multilayered thin film with N = 16. The peaks at 2θ ≈ 21.98, 22.30, and 22.94° were identified as the satellite peaks. For N = 16, the thickness of every periodic layer (L) is about 30 nm, giving the multilayered film thickness is about 480 nm. Moreover, the L for the N = 30 obtained is about 17 nm, giving the thickness of about 510 nm. This value is somewhat about 10% larger than the designed structure, probably due to the partial strain released in the hetero-structures The results were calculated from the θ-2θ scans employed the standard formula[38] $L = [\lambda_{Cu(K\alpha)}/(\sin\theta_{m+1} - \sin\theta_m)]$, where $\lambda_{Cu(K\alpha)}$ is the wavelength of the Cu($K\alpha$) radiation and m corresponds to the mth satellite peak. The visible satellite peaks in the large periodic number N are resulted from the fact that the smaller L cause the larger separation of θ_{m+1} and θ_m because the larger the periodic number N the smaller the layer thickness in the combinations.

The ϕ scans have been done to understand the epitaxial quality and the in-plane texture between the multilayered thin films and the substrates. Figure 2c shows the ϕ scans taken from the {101} planes of the multilayered thin films and MgO substrates, displaying that only a clear 4-fold symmetry peaks from {101} reflections were presented in the scans. The in-plane interface relationship between the multilayered thin films and the MgO substrate can be determined to be $[001]_{STO}//[001]_{BTO}//[001]_{MgO}$ and $(100)_{STO}//(100)_{BTO}//(100)_{MgO}$.

To better understand the epitaxial quality of the as-grown multilayered thin films, the cross-sectional TEM studies have been employed to further investigate the epitaxial behavior and interface microstructure of the BTO/STO multilayered thin films (N=30) on (001) MgO substrates. Figure 3a is a bright-field TEM image, showing columnar-like structure features and a clear sharp interface between the multilayered thin films and the substrate. The film thickness is determined to be 465 nm, which is close to the designed structure value, and the X-ray diffraction calculation value of 510 nm. Figure 3b is a selected area electron diffraction (SAED) pattern taken from the multilayered BTO/STO film regions. It shows a single crystal electron diffraction pattern. Diffraction spots are sharp for those with lower indices but are broadened for those with higher indices. The broadening of the higher order diffraction spots may be due to the smaller orientation variation of the grains. The lattice mismatch between the BTO and STO is too small to be shown on the electron diffraction pattern in Figure 3b. Figure 3c is a SAED pattern taken from the multilayered film and the MgO substrate interface showing an epitaxial growth of the multilayered films. The lattice mismatch between the multilayered film and the substrate determined from this SAED pattern is ∼ −6.8%. The orientation relationship between the multilayered BTO/STO films and the MgO substrate is $(001)_{BTO}//(001)_{STO}//(001)_{MgO}$ and $[100]_{BTO}//[100]_{STO}//[100]_{MgO}$. Cross-sectional high-resolution TEM (HRTEM) has further demonstrated the epitaxial growth of the multilayered films on MgO substrate, Figure 3d, e. Figure 3d shows that the films have an epitaxial behavior with a sharp and flat interface structure with respect to the substrate. Figure 3e shows that an atomically sharp interface was also formed between the BTO and STO layers.

Figure 4 shows the values of the dielectric constant and loss tangent measured at ∼18 GHz and room temperature as a function of the N. The dielectric constants dramatically increase with the increase of the N and the dielectric loss tangent also rapidly decrease with the increase of the N. The optimized dielectric properties determined with the low dielectric loss tangent (0.02) at high frequency is achieved at $N \geq 16$ with the dielectric constant (1320). It is interesting to note that when the periodic number is less than 16 (both 4 and 8 combinations), the heterostructures have the performances similar to the dielectric constant of STO and the dielectric loss of BTO. In fact, this can be understood by considering that the heterostructures are the serial combinations of BTO and STO systems. In the dielectric property measurements, the dielectric constant is domestically contributed from the small dielectric constant capacitance STO layers system in the serial combination system but the dielectric loss is from the large dielectric loss BTO layers system. Therefore, the dielectric constant and the dielectric loss of the heterostructures are dependent on the STO layers and the BTO layers, respectively. However, a transition occurs when the period number is larger than 16, where a dielectric response similar to that of the ceramic $(Ba,Sr)TiO_3$ thin films is observed with a much lower dielectric loss. More exactly to say, when each ferroelectric STO layer thickness in the heterostructures is less than 6 nm, the dielectric constants are similar to those of their ceramic $(Ba,Sr)TiO_3$ thin films but have much lower dielectric losses. These results indicate that the interface and nanostructure effects play important key roles in these nanolayered heterostructures systems. These phenomena can also be understood from the X-ray diffraction characterization where the satellite peaks start to show up when the combination

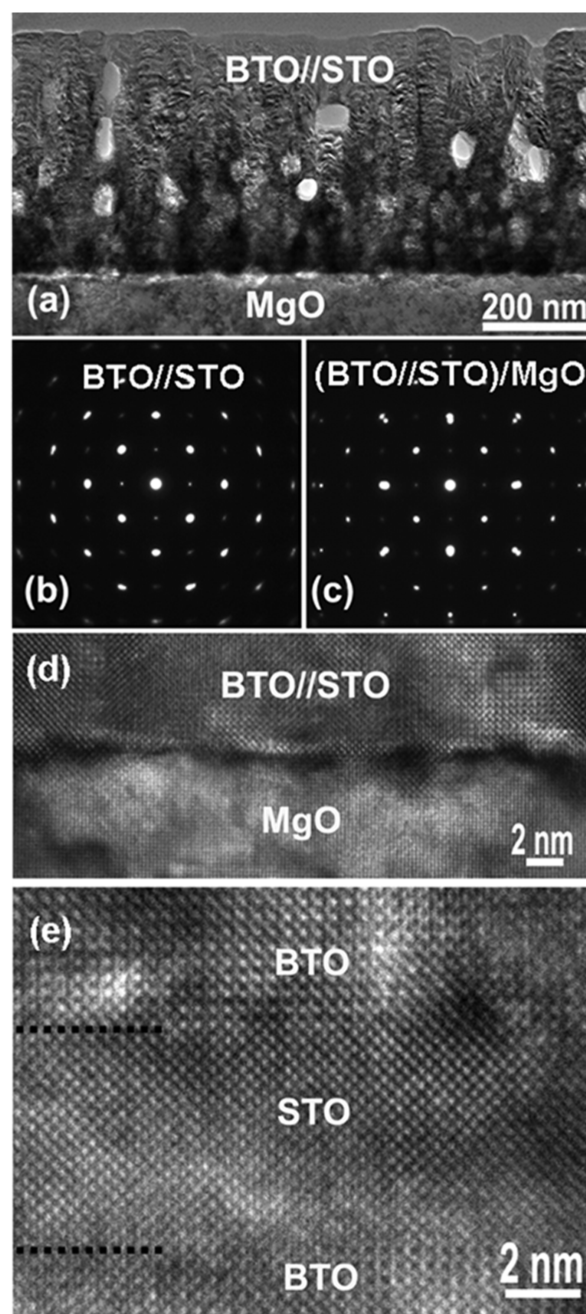

Figure 3. Cross-sectional TEM studies showing the epitaxial behavior of as-grown BTO//STO multilayered thin films on (001) MgO. (a) Low-magnification, bright-ield TEM image, (b) SAED from film, (c) SAED from the interface covering both film and MgO substrate, (d) high-resolution image showing the interface structure and epitaxial behavior between the film and the substrate, (e) an atomically sharp interface between the BTO and STO layers.

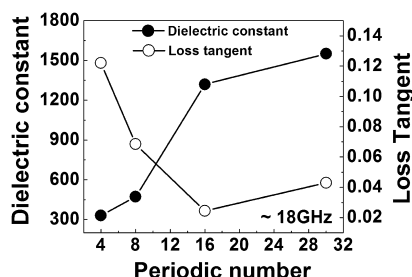

Figure 4. *N* dependent on the value of the dielectric conastant and the loss tangent of the as-grown BTO/STO multilayered thin films on MgO substrates.

number is larger than 16. The agreement between the X-ray diffraction characterization and microwave dielectric measurement indicates the strong interface effects occurred in the systems when $N \geq 16$. The nature of the interface effects and nanostructure performance in the BTO/STO heterostructures is under investigation and will be reported later. It should be pointed out here that the extra low dielectric loss behavior suggests that the BTO/STO multilayered thin films can be used to develop for room-temperature microwave elements.

CONCLUSIONS

In summary, ferroelectric BTO/STO heterostructures have been epitaxially grown on (001) MgO by pulsed laser deposition. The microstructure studies from the X-ray diffraction and transmission electron microscopy indicated that the films are highly *c*-axis oriented and have atomic sharp interface. The interface relationships were determined to be $[001]_{BTO}//[001]_{STO}//[001]_{MgO}$ and $(100)_{BTO}//(100)_{STO}//(100)_{MgO}$. The high-frequency microwave (~18 GHz) dielectric measurements reveal that the dielectric constant and loss tangent of the films are varying with the stacking period number. The optimized dielectric performance determined by the value for the loss tangent (0.02) is achieved at N=16 with the dielectric constant (1320). The strong interface effect and nanostructure interaction were found when the combination period is larger than 15, or each STO layer is less than 6.0 nm. The ultra low dielectric loss performance in the microwave frequency suggests that the interface engineered BTO/STO heterostructures can be developed for the room-temperature microwave element applications.

AUTHOR INFORMATION

Corresponding Author

*E-mail: cl.chen@utsa.edu.

Notes

The authors declare no competing financial interest.

ACKNOWLEDGMENTS

This research was partially supported by the National Science Foundation under NSF-NIRT-0709293, the State of Texas through the ARP Program under 003656-0103-2007 and the Texas Center for Superconductivity at the University of Houston, and the Natural Science Foundation of China under 11028409. Also, M.L. and C.M. acknowledge the support from the "China Scholarship Council" for the program of national study-abroad project for the postgraduates of high level universities at UTSA.

REFERENCES

(1) Scott, J. F. *Annu. Rev. Mater. Sci.* **1998**, *28*, 79−100.
(2) Tagantsev, A. K.; Sherman, V. O.; Astafiev, K. F.; Venkatesh, J.; Setter, N. *J. Electroceram.* **2003**, *11*, 5−66.
(3) Liu, M.; Ma, C. R.; Collins, G.; Liu, J.; Chen, C. L.; Shui, L.; Wang, H.; Dai, C.; Lin, Y.; He, J.; Jiang, J. C.; Meletis, E. I.; Zhang, Q. Y. *Cryst. Growth Des.* **2010**, *10*, 4221−4223.
(4) Gan, Y.; Cai, Q. J.; Li, C. M.; Yang, H. B.; Lu, Z. S.; Gong, C.; Chan-Park, M. B. *ACS Appl. Mater. Interfaces* **2009**, *1*, 2230−2236.
(5) Lin, Y.; Chen, C. L. *J. Mater. Sci.* **2009**, *44*, 5274.
(6) Zhou, T.; Zha, J. W.; Cui, R. Y.; Fan, B. H.; Yuan, J. K.; Dang, Z. M. *ACS Appl. Mater. Interfaces* **2011**, *3*, 2184−2188.
(7) Wang, G. S. *ACS Appl. Mater. Interfaces* **2010**, *2*, 1290−1293.
(8) Liu, M.; Liu, J.; Collins, G.; Ma, C. R.; Chen, C. L.; Alemayehu, G.; Subramanyam, G.; Dai, C.; Lin, Y.; He, J.; Jiang, J. C.; Meletis, E. I.; Zhang, Q. Y. *J. Adv. Dielectr.* **2011**, *1*, 383−387.
(9) Liu, S. W.; Weaver, J.; Donner, W.; Yuan, Z.; Chen, C. L.; Jiang, J. C.; Meletis, E. I.; Chang, W.; Kirchoefer, S. W.; Horwitz, J.; Bhalla, A. *Appl. Phys. Lett.* **2005**, *87*, 142905.
(10) Chen, C. L.; Shen, J.; Chen, S. Y.; Luo, G. P.; Chu, C. W.; Miranda, F. A.; Van Keuls, F. W.; Jiang, J. C; Meletis, E. I; Chang, H. Y. *Appl. Phys. Lett.* **2001**, *78*, 652−654.
(11) Carlson, C. M.; Rivkin, T. V.; Parilla, P. A.; Perkins, J. D.; Ginley, D. S.; Kozyrev, A. B.; Oshadchy, V. N.; Pavlov, A. S. *Appl. Phys. Lett.* **2000**, *76*, 1920−1922.
(12) Chen, C. L.; Chen, H. H.; Zhang, Z.; Brazdeikis, A.; Huang, Z. J.; Chu, W. K.; Chu, C. W.; Miranda, F. A.; Van Keuls, F. W.; Romanofsky, R. R.; Liou, Y. *Appl. Phys. Lett.* **1999**, *75*, 412−414.
(13) Kim, W. J.; Chang, W.; Qadri, S. B.; Pond, M. J.; Kirchoefer, S. W.; Chrisey, D. B.; Horwitz, J. S. *Appl. Phys. Lett.* **2000**, *76*, 1185−1187.
(14) Zhong, S.; Alpay, S. P.; Cole, M. W.; Ngo, E.; Hirsch, S.; Demaree, J. D. *Appl. Phys. Lett.* **2007**, *90*, 2092901.
(15) Lin, Y.; Lee, J. S.; Wang, H.; Li, Y.; Foltyn, S. R.; Jia, Q. X.; Collis, G. E.; Burrel, A. K.; McCleskey, T. M. *Appl. Phys. Lett.* **2004**, *785*, 5007−5009.
(16) Tian, W.; Jiang, J. C.; Pan, X. Q.; Haeni, J. H.; Li., Y. L.; Chen, L. Q.; Schlom, D. G.; Neaton, J. B.; Rabe, K. M.; Jia, Q. X. *Appl. Phys. Lett.* **2006**, *89*, 092905.
(17) Chang, W. T.; Horwitz, J. S.; Cater, A. C.; Pond, J. M.; Kirchoefer, S. W.; Gilmore, C. M.; Chrisey, D. B. *Appl. Phys. Lett.* **1999**, *74*, 1033−1035.
(18) Moon, S. E.; Kim, E. K.; Kwak, M. H.; Ryu, H. C.; Kim, Y. T. *Appl. Phys. Lett.* **2003**, *83*, 2166−2168.
(19) Cole, M. W.; Joshi, P. C.; Ervin, M. H.; Wood, M. C.; Pfeffer, R. L *Thin Solid Films* **2000**, *374*, 34−41.
(20) Jain, M.; Majumder, S. B.; Katiyar, R. S.; Agrawal, D. C.; Bhalla, A. S. *Appl. Phys. Lett.* **2002**, *81*, 3212−3214.
(21) Alldredge, L. M. B.; Chang, W.; Kirchoefer, S. W.; Pond, J. M. *Appl. Phys. Lett.* **2009**, *95*, 222902.
(22) Cole, M. W.; Weiss, C. V.; Ngo, E.; Hirsch, S.; Coryell, L. A.; Alpay, S. P. *Appl. Phys. Lett.* **2008**, *92*, 182906.
(23) Yuan, Z.; Lin, Y.; Weaver, J.; Chen, X.; Chen, C. L.; Subramanyam, G.; Jiang, J. C.; Meletis, E. I. *Appl. Phys. Lett.* **2005**, *87*, 152901.
(24) Stephanovich, V. A.; Luk'yanchuk, I. A.; Karkut, M. G. *Phys. Rev. Lett.* **2005**, *94*, 047601.
(25) Okatan, M. B.; Misirlioglu, I. B.; Alpay, S. P. *Phys .Rev. B* **2010**, *82*, 094115.
(26) Misirlioglu, I. B.; Pintilie, L.; Boldyreva, K.; Alexe, M.; Hesse, D. *Appl. Phys. Lett.* **2007**, *91*, 202905.
(27) Speche, E. D.; Chritem, H. −M.; Norton, N. D.; Boatner, L. A. *Phys. Rev. Lett.* **1998**, *80*, 4317−4320.
(28) Sepliarsky, M.; Phillpot, S. R.; Wolf, D.; Stachiotti, M. G.; Migoni, R. L. *Phys. Rev. B* **2001**, *64*, 060601(R).
(29) Sepliarsky, M.; Stachiotti, M. G.; Migoni, R. L. *Phys. Rev. Lett.* **2006**, *96*, 137603.
(30) Jang, H. W.; Kumar, A.; Denev, S.; Biegalski, M. D.; Maksymovych, P.; Bark, C. W.; Nelson, C. T.; Folkman, C. M.;

Folkman, C. M.; Balke, N.; Brooks, C. M.; Tenne, D. A.; Schlom, D. G.; Chen, L. Q.; Pan, X. Q.; Kalinin, S. V.; Gopalan, V.; Eom, C. B. *Phys. Rev. Lett.* **2010**, *194*, 197601.
(31) Nakagawara, O.; Shimuta, T.; Makino, T.; Arai, S. *Appl. Phys. Lett.* **2000**, *77*, 3257−3259.
(32) Lee, J.; Kim, L.; Kim, J.; Jung, D.; Waghmare, U. V. *J. Appl. Phys.* **2006**, *100*, 051613.
(33) Tabata, H.; Tanaka, H.; Kawai, T. *Appl. Phys. Lett.* **1994**, *65*, 1970−1972.
(34) Kim, L.; Jung, D. G.; Kim, J.; Kim, Y. S.; Lee, J. *Appl. Phys. Lett.* **2003**, *82*, 2118−2120.
(35) Kim, J.; Kim, Y.; Kim, Y. S.; Lee, J.; Kim, L.; Jung, D. *Appl. Phys. Lett.* **2002**, *80*, 3581−3583.
(36) Krupka, J.; Breeze, J.; Centeno, A.; Alford, N.; Claussen, T.; Jensen, L. *IEEE Trans. Microwave Theory Tech.* **2006**, *54*, 3995−4001.
(37) Krupka, J. *Meas. Sci. Technol.* **2006**, *17*, 55−70.
(38) Marre, L. E.; Farhi, R.; Marssi, M. E.; Lukyanchuk, I. A.; Karkut, M. G. *J. Appl. Phys.* **2003**, *94*, 3307−3312.